Bulletin of the Seismological Society of America, 91, 6, pp. 1924–1929, December 2001

Modeling Anomalous Surface-Wave Propagation across the Southern Caspian Basin

by Keith Priestley, Howard J. Patton, and Craig A. Schultz

Abstract The South Caspian Basin contains one of the thickest sedimentary deposits in the world. Intermediate-frequency (0.02–0.04 Hz) fundamental-mode Rayleigh waves propagating across the basin are severely attenuated, but apparent attenuation is significantly less for both low and high frequencies. We have modeled the response of surface waves in a simplified rendition of the South Caspian Basin model of Mangino and Priestley (1998) using a hybrid normal-mode/2D finite-difference approach. To gain insight into the features of the basin that cause the anomalous surface-wave propagation, we have varied parameters of the basin model and computed synthetic record sections to compare with the observed seismograms. We have varied the Moho depth beneath the basin, the shape of the basin boundaries, the thickness and shear-wave Q of the sediments and mantle, and the water depth. Of these parameters, the intermediate-frequency surface waves are most severely affected by the sediment thickness and shear-wave attenuation. All models fail to satisfy observations for frequencies of 0.05 Hz and above, and this failure is attributed to significant 3D wave propagation effects caused by focusing and scattering of surface waves by basin structures.

Introduction

Kadinsky-Cade *et al.* (1981) demonstrate that *Lg* is blocked for paths crossing the South Caspian Basin but propagates efficiently in the surrounding region. On the other hand, *Sn* propagates efficiently for paths across the South Caspian but poorly in the region south and west of the basin. *Lg* is sensitive to changes in crustal structure along its propagation path and the phase is absent in seismograms after propagating across about 150 km of oceanic crust (Press and Ewing, 1952). The efficient propagation of *Sn* and the blockage of *Lg* have been cited as evidence that the South Caspian Basin is floored by oceanic crust.

New seismic data from this region show that intermediate-frequency fundamental-mode surface waves propagating across the South Caspian Basin are also severely attenuated. In many cases, the recordings on the near side of the basin show well-dispersed surface waveforms whereas recordings on the far side of the basin are deficient in intermediate-frequency (0.02–0.04 Hz) surface waves. There are several instances where the stations LNK and KAT (Fig. 1) lie along the same great circle path for an earthquake and the anomalous effect of propagation across the basin is particularly clear. Figure 1 shows vertical component seismograms for two earthquakes whose epicenters lie on the same great circle path as LNK and KAT. The upper pair of seismograms are waves propagating along a great circle path between KAT and LNK from an earthquake in Timor; the lower pair of seismograms are waves propagating along a great circle path between LNK and KAT from an earthquake on the Mid-Atlantic Ridge. All waveforms are plotted on the same amplitude scale. Both events show a well-developed surface-wave-train entering the basin, but the intermediate-frequency surface waves are greatly reduced in amplitude on the far side of the basin only 450 km away. The amplitude reduction in the 25–33-sec period range translates into a Rayleigh-wave quality factor, Q_R, of about 35, significantly lower than estimates of Q_R ($\sim$60) for the Basin and Range (Patton and Taylor, 1984). Shorter periods yield Q_R of about 120, comparable to estimates for the Basin and Range. Because strong attenuation is observed for both eastward- and westward-propagating surface waves across the South Caspian Basin, the erosion of intermediate-frequency surface waves is unlikely to be a result of a site or instrumental effect.

The South Caspian Basin has a very unusual velocity structure (Mangino and Priestley, 1998). In this study, we examine the effect of this velocity structure on the propagation of surface waves by computing finite-difference (FD) synthetic seismograms for a simplified 2D crustal model of the South Caspian Basin. We then vary the crustal and upper-mantle parameters of the simplified model and recompute the synthetic seismograms to determine which parameters of this 2D model have the greatest influence the

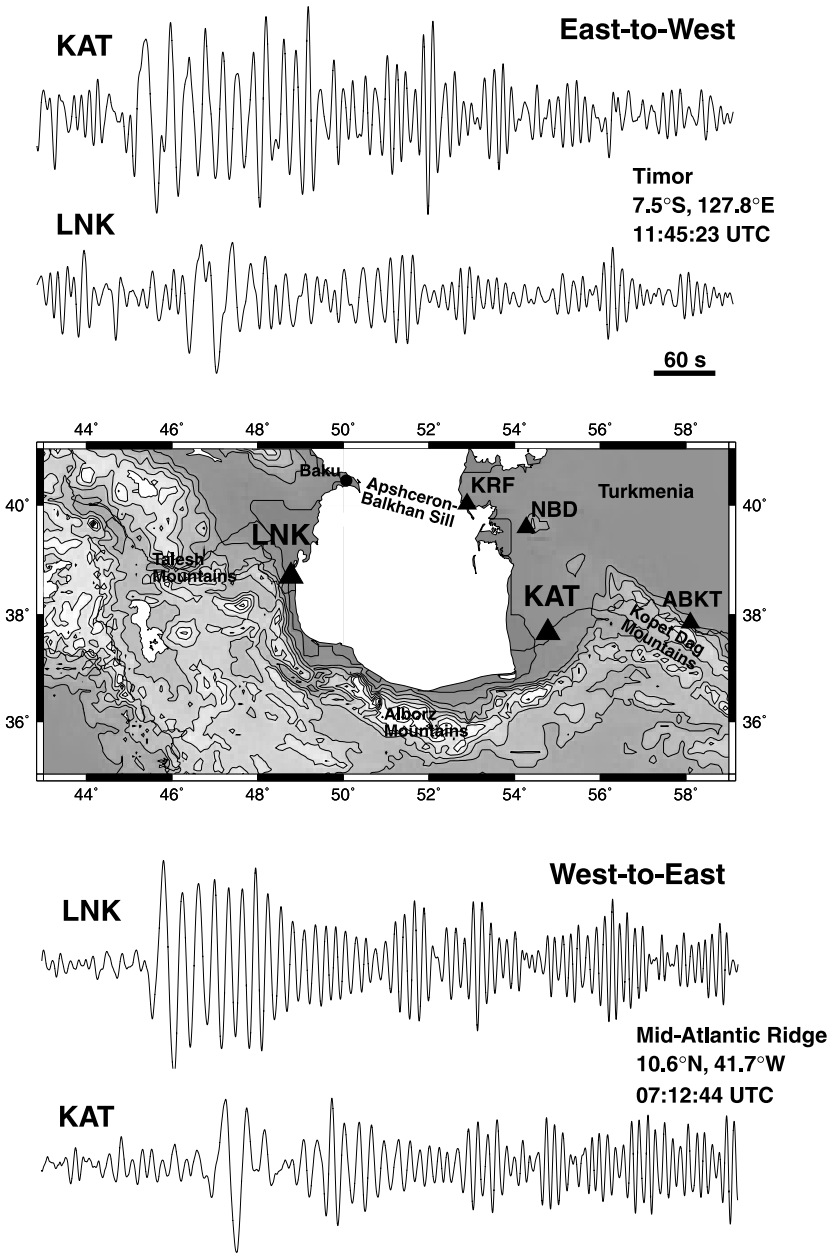

Figure 1. The middle part of the figure shows a map with locations of the broadband digital stations in the region surrounding the South Caspian basin. Seismograms for two earthquakes lying on the same great circle path as the stations are shown above and below the map. The lower pair of seismograms are from an earthquake on the Mid-Atlantic Ridge; the upper pair of seismograms are from an earthquake in Timor. All seismograms are plotted at the same amplitude scale.

surface-wave propagation across the basin. Whereas 2D models can satisfy the observations at intermediate frequencies, we find that significant 3D effects must play a role at frequencies above 0.05 Hz.

Modeling Anomalous Surface-Wave Propagation

Mangino and Priestley (1998) combined receiver-function analysis results from broadband teleseismic seismograms recorded around the South Caspian Basin and published seismic refraction results to produce the velocity model for the southern Caspian shown in Figure 2a. The crust in Turkmenia along the trend of the Apshceron-Balkhan Sill-Kopet Dag Mountains (Fig. 1, KRF, NBD, and ABKT) is about 50 km thick. In the southwestern part of the Caspian basin (Fig. 1, LNK) the 33-km-thick crust consists of a 13-km-thick sedimentary section lying on a high-velocity ($V_p \sim 7.1$ km sec^{-1}) lower-crustal section. In the southeastern part of the basin (Fig. 1, KAT) the crust is 30 km thick and consists of a 10-km-thick sedimentary section overlying a 20-km-thick low velocity ($V_p \sim 5.8$ km sec^{-1}) crystalline crust. The most significant features of the crustal model in Figure 2a are the 20-km variation in thickness of Cenozoic sedimentary basin deposits, the absence of a *granitic* ($V_p \sim 5.8$–6.5 km sec^{-1}) crustal layer in the central part of the South Caspian Basin, and 20 km of crustal thinning beneath the central part of the basin. The Moho beneath the South Caspian Basin has a broad arch-like structure whose

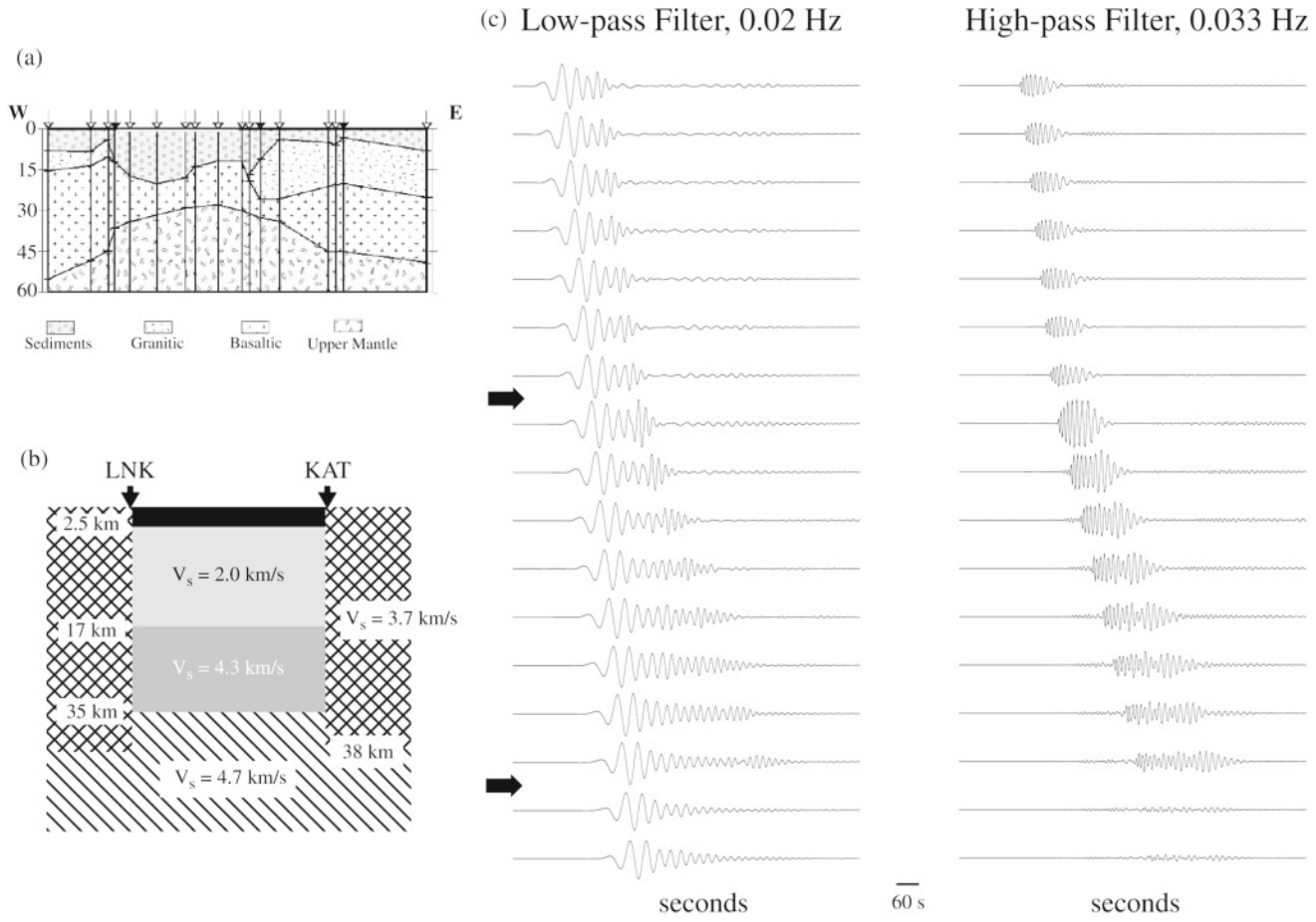

Figure 2. (a) The South Caspian basin model of Mangino and Priestley (1998). (b) The simplified South Caspian basin shear-wave model used in the FD calculations. (c) Synthetic surface-wave record sections for two passbands: up to 0.02 Hz at left, and 0.033 Hz and above at right. The large arrows denote the location of the basin boundaries. All seismograms in a record section are plotted at the same amplitude scale, but the two record sections have different scales.

western boundary is a relatively narrow zone across which the crust thins rapidly (~20 km thinning over a 100-km zone) and whose eastern boundary has a more gradual change in crustal thickness (~20 km thinning over a 400-km zone).

The anomalous surface-wave propagation across the South Caspian Basin could possibly result from a number of the extreme structural features of the basin. To isolate the features responsible for the anomalous surface-wave propagation, we have computed 2D FD seismograms for a simplified model of the South Caspian Basin and the surrounding region (Fig. 2b and Table 1) that emulates the main features of the velocity model shown in Figure 2a. This is the reference model in the comparisons discussed subsequently. The background model is 900-km wide by 450-km deep and is gridded at a 1.05-km interval in both distance and depth. The basin lies between 381 and 761 km from the left edge of the grid. Inputs at the left edge of the FD grid are the stresses and displacements as functions of depth for fundamental-mode Rayleigh waves excited by a 12-km-deep explosion source located 2000 km away. These were generated by a normal-mode synthetic seismogram code. Although all of the events observed are earthquakes, we have used an explosion source for simplicity in the simulations. Receivers are placed at 50-km intervals across the model and are located on the solid surface, that is, in those models with a water layer, the receivers are placed at the water-solid

Table 1

Model	Thickness (km)	V_p (km s^{-1})	V_s (km s^{-1})	ρ (gm cm^{-3})	Q_p	Q_s
Background model	38.0	6.40	3.70	2.82	∞	∞
	450.5	8.13	4.70	3.37	∞	∞
Basin model	2.625	1.51	0.00	1.00	∞	∞
	14.375	3.46	2.00	1.88	100	50
	16.000	7.44	4.30	3.15	1000	500

interface. The seismograms are computed with 20,000 time steps of 0.075 sec each.

Figure 2c shows the vertical component synthetic seismograms at intervals of 50 km across the reference model in two passbands: less than 0.020 and greater than 0.033 Hz. The basin effect on the wave train is most pronounced on the high-frequency waves, but the basin-structure effect is also apparent for low frequencies. The high-frequency wave train shows an increased amplitude after entering the basin, a result of the impedance mismatch across the basin boundary. Small-amplitude converted body waves propagate into the basin and, along with reflected surface waves, propagate back toward the left edge of the model. The amplitudes of these waves are too small to be seen at the amplitude scale used in Figure 2c. The duration of the surface-wave train increases during propagation across the basin due to the increased dispersion resulting from the thick, low-velocity sediments. High-frequency surface waves reverberate in the basin at large travel times. The high-pass surface-wave amplitudes are reduced after the wave train passes out of the basin and enters the more rigid material on the right side of the basin. The highest-frequency components in the low-frequency passband are also amplified upon entering the basin as well as reflected back toward the left edge of the model. Surface waves of these frequencies are affected by the increased dispersion across the basin and are attenuated on passing out of the basin. The lowest-frequency component shows little effect of the basin structure.

To isolate the features that most contributed to the anomalous surface-wave propagation, we perturbed the basin model velocity and attenuation structure in a number of ways and compared synthetic seismograms computed for these models with those computed for the reference model. Most of the structural features of the basin such as the thickness of the crystalline crust beneath the basin, degree of mantle upward beneath the basin, shape of the basin boundaries, and so on have little effect on the synthetic seismograms compared with the seismograms of the reference model. The features that significantly influence the surface waveforms are the sediment thickness and the attenuation structure of the basin. The results are shown in Figure 3. This compares the observed fundamental-mode Rayleigh-wave spectral ratio between stations KAT and LNK with the spectral ratios of various FD models. Increasing the sediment thickness to 22.4 km (model A in Fig. 3) or decreasing the sediment Q to 10 (model B) attenuates the high-frequency surface waves but does not quite match the high attenuation of the data in the 0.025- to 0.04-Hz band. Increasing attenuation in the mantle beneath the basin (model C) reduces the intermediate period amplitudes, but this model is inconsistent with results showing normal upper mantle *P*- and *S*-wave velocities beneath the South Caspian Basin (Priestley *et al.,* 2000). Extending the basin sediments beneath the observation points representing KAT and LNK in the FD 2D models causes a small resonance peak near 0.04 Hz, which is not present in the observations. In summary, none of the FD models we tested were able to reduce the energy in the intermediate period band on synthetic seismograms to the degree seen in the KAT-LNK seismograms, nor were the models able to reproduce the frequency dependence of amplitude ratios above 0.04 Hz.

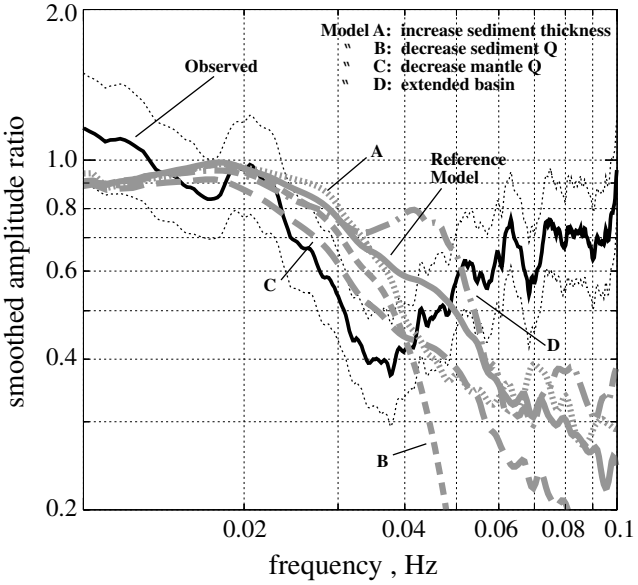

Figure 3. Amplitude ratios for Rayleigh waves propagating across the South Caspian Sea. Black line and thin dotted lines are the average ratio and one-standard-deviation error bars based on 14 sets of observations for stations KAT and LNK. Thick gray lines are amplitude ratios from FD modeling: (1) solid-reference model, (2) dotted-model A, (3) short dash-model B, (4) long dash-model C, and (5) dash-dot-model D.

Discussion and Conclusions

All of the FD models we tried have axes of symmetry about the center of the basin so that it did not matter which direction the surface waves propagated, west to east or east to west. Such models were chosen to reduce the complexity of the analysis, but in the real basin, structures on either side of and beneath the South Caspian Sea are asymmetric. Whereas attenuation of intermediate-period surface waves is largely controlled by sediments in the basin, the mismatch between the predictions of the FD models and the observations in Figure 3 could be related to the fact that our FD models did not account for structural details near the recording stations KAT and LNK. This is relevant because the observations are heavily weighted by data for east-to-west propagation (KAT to LNK, 14 events; LNK to KAT, 1 event). A data set composed of equal sampling of both eastward- and westward-propagating waves would have mitigated potential receiver-site effects.

We performed a simple calculation of surface-wave medium responses to illustrate qualitatively that differences in

Earth structures local to KAT and LNK can explain the mismatch of FD models for intermediate periods. According to Saito (1967) the surface-wave medium response in 1D structures is proportional to $1/CUI_1$, where C is phase velocity, U is group velocity, and I_1 is kinetic energy of the eigenfunction for a particular normal mode. Medium responses were computed using the layered models KAT-ESE and LNK-ENE of Mangino and Priestley (1998) and the ratio between these responses is plotted in Figure 4. The ratio shows that the responses are nearly equal for frequencies below 0.02 Hz; they differ the most above 0.05 Hz, and a transition regime exists between 0.02 and 0.05 Hz.

Thus, the medium responses predict that fundamental-mode Rayleigh-wave amplitudes are larger in the structure local to KAT compared with LNK, but the differences only become appreciable above 0.02 Hz. The frequency dependence of the ratio in the transition mimics the mismatch of FD models in Figure 3 fairly well between 0.02 and 0.04 Hz and with approximately the required amplitude (to correct the FD predictions, the response ratio in Fig. 4 must be divided into the FD ratios). Although the comparison for intermediate frequencies improves with this correction, the model predictions degrade significantly at higher frequencies. Indeed, most models overpredict the amount of attenuation by at least a factor of 5 for frequencies of 0.05 Hz and above.

We believe the failure to predict amplitude ratios above 0.05 Hz is caused by effects of 3D wave propagation in the observations, probably related to focusing of surface-wave energy by large-scale basin structures and scattering off small-scale heterogeneities. The difference between medium responses for frequencies of 0.05 Hz and above (Fig. 4) is merely one indication that lateral variations of structures are likely to have increasing adverse effects on the propagation of short-period surface waves through the South Caspian Sea region. Varied geological structures of the region offer another indication: witness the Talesh mountains forming the western boundary, the Alborz mountains the southern boundary, and the Kopet Dag and Alborz mountains the eastern boundary. The Apshceron-Balkan sill, a seismically active shallow ridge separating the northern and southern Caspian, makes up the northern boundary of the South Caspian Basin. The increased effect of 3D structure at increasing frequency implies that the pronounced effect the South Caspian Basin has on the *Lg* phase will not be explained by 2D simulations.

The South Caspian Sea is an actively subsiding basin with extremely high rates of Cenozoic sedimentation, in some places as high as 1300 m m.y.$^{-1}$ Figure 2a shows that the basin contains as much as 25 km of sediment in the deepest parts. Borehole data in the Caspian Sea south of Baku show that these sediments consist of both sand and shale beds that have pore-fluid pressure substantially in excess of hydrostatic fluid pressure and this condition exists to at least 5-km depth (Bredehoeft *et al.,* 1988). This high pore-fluid pressure is the likely cause of the large number of mud volcanos found along the coast and on the bed of the South Caspian Sea, and their widespread occurrence indicates that the overpressured sediments occur over most, if not all, of the basin. The thick sediments in the sea have a pronounced effect on the propagation of surface waves across the basin for frequencies of 0.02 Hz and above. We have used a hybrid normal-mode-finite-difference code and a simplified model of the South Caspian Basin to study the relative contribution of basin features to the anomalous surface-wave propagation. Variations in the velocity of the crystalline crust of the basin and in the mantle upwarp beneath the basin result in a small part of the surface-wave energy being converted into body waves and being lost, but on the whole these features have little effect on the intermediate-frequency surface waves. In contrast, the thick, highly attenuating sediments do have a significant effect on the surface waveform. This results from (1) the increased high-frequency dispersion, which gives an apparent decrease in amplitude by stretching the waveform out in time; and (2) the high attenuation of the sediments, which has a large effect on the high-frequency surface waves but little effect on the low-frequency surface waves. However, consideration of 3D structure will be required to explain propagation of high-frequency (>0.04 Hz) surface waves.

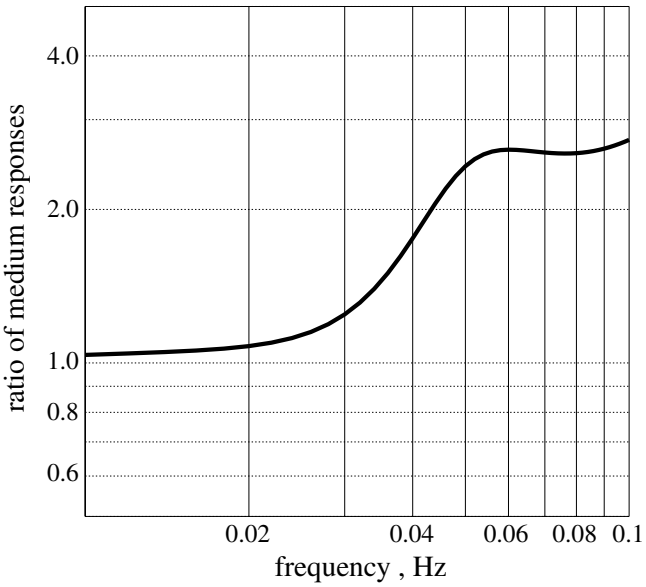

Figure 4. Ratio of 1D medium responses for fundamental-mode Rayleigh waves based on the receiver-function models, KAT-ESE and LNK-ENE, of Mangino and Priestley (1998).

Acknowledgments

We would like to thank Steve Mangino and Mikhail Rozhkov for their efforts in the field experiment, which obtained the Caspian data. We would also like to thank Shawn Larsen for the use of his finite-difference wave-propagation code. The work of HJP and CAS was supported under the auspices of the Department of Energy by the Los Alamos and Lawrence Livermore National Laboratories under Contracts W-7405-ENG-36 and

W-7405-ENG-48, respectively. This is Cambridge University Department of Earth Sciences Contribution No. 6491 and Los Alamos Seismic Research Center Contribution No. 0016.

References

Bredehoeft, J. D., R. D. Djevanshir, and K. R. Belitz (1988). Lateral fluid flow in a compacting sand-shale sequence: South Caspian basin, *Am. Assoc. Pet. Geol. Bull.* **72,** 416–424.

Kadinsky-Cade, K., M. Barazangi, J. Oliver, and B. Isacks (1981). Lateral variations of high-frequency seismic wave propagation at regional distances across the Turkish and Iranian Plateaus, *J. Geophys. Res.* **86,** 9377–9396.

Mangino, S., and K. Priestley (1998). The crustal structure of the southern Caspian region, *Geophys. J. Int.* **133,** 630–648.

Patton, H. J., and S. R. Taylor (1984). *Q* structure of the Basin and Range from surface waves, *J. Geophys. Res.* **89,** 6929–6940.

Press, F., and M. Ewing (1952). Two slow surface waves across North America, *Bull. Seism. Soc. Am.* **42,** 219–228.

Priestley, K., H. J. Patton, and C. Schultz (2000). Crust and upper mantle seismic structure of the south Caspian basin (abstract), *Seism. Res. Lett.* **71,** 259.

Saito, M. (1967). Excitation of free oscillations and surface waves by a point source in a vertically heterogeneous Earth, *J. Geophys. Res.* **72,** 3689–3699.

Bullard Laboratories
Madingley Rise, Madingley Road
Cambridge CB3 0EZ
U.K.
keith@esc.cam.ac.uk
(K.P.)

Los Alamos Seismic Research Center
Los Alamos National Laboratory
Los Alamos, New Mexico 87545
patton@lanl.gov
(H.J.P.)

Geophysics and Global Security
Lawrence Livermore National Laboratory
Livermore, California 94551
cschultz@llnl.gov
(C.A.S.)

Manuscript received 10 February 2001